Tumor and Stem Cell Biology

Cancer Research

CRISPR/Cas9-Mediated *Trp53* and *Brca2* Knockout to Generate Improved Murine Models of Ovarian High-Grade Serous Carcinoma

Josephine Walton[1,2], Julianna Blagih[3], Darren Ennis[1], Elaine Leung[1], Suzanne Dowson[1], Malcolm Farquharson[1], Laura A. Tookman[4], Clare Orange[5], Dimitris Athineos[3], Susan Mason[3], David Stevenson[3], Karen Blyth[3], Douglas Strathdee[3], Frances R. Balkwill[2], Karen Vousden[3], Michelle Lockley[4], and Iain A. McNeish[1,4]

Abstract

There is a need for transplantable murine models of ovarian high-grade serous carcinoma (HGSC) with regard to mutations in the human disease to assist investigations of the relationships between tumor genotype, chemotherapy response, and immune microenvironment. In addressing this need, we performed whole-exome sequencing of ID8, the most widely used transplantable model of ovarian cancer, covering 194,000 exomes at a mean depth of 400× with 90% exons sequenced >50×. We found no functional mutations in genes characteristic of HGSC (*Trp53*, *Brca1*, *Brca2*, *Nf1*, and *Rb1*), and p53 remained transcriptionally active. Homologous recombination in ID8 remained intact in functional assays. Further, we found no mutations typical of clear cell carcinoma (*Arid1a*, *Pik3ca*), low-grade serous carcinoma (*Braf*), endometrioid (*Ctnnb1*), or mucinous (*Kras*) carcinomas. Using CRISPR/Cas9 gene editing, we modeled HGSC by generating novel ID8 derivatives that harbored single ($Trp53^{-/-}$) or double ($Trp53^{-/-}$;$Brca2^{-/-}$) suppressor gene deletions. In these mutants, loss of p53 alone was sufficient to increase the growth rate of orthotopic tumors with significant effects observed on the immune microenvironment. Specifically, p53 loss increased expression of the myeloid attractant CCL2 and promoted the infiltration of immunosuppressive myeloid cell populations into primary tumors and their ascites. In $Trp53^{-/-}$;$Brca2^{-/-}$ mutant cells, we documented a relative increase in sensitivity to the PARP inhibitor rucaparib and slower orthotopic tumor growth compared with $Trp53^{-/-}$ cells, with an appearance of intratumoral tertiary lymphoid structures rich in $CD3^+$ T cells. This work validates new CRISPR-generated models of HGSC to investigate its biology and promote mechanism-based therapeutics discovery. *Cancer Res; 76(20); 6118–29. ©2016 AACR.*

Introduction

Ovarian high-grade serous carcinoma (HGSC) is the commonest subtype of human ovarian cancer (1), and long-term survival remains poor (2). Mutation in *TP53* is essentially universal (3, 4), whereas germline mutation in *BRCA1* or *BRCA2* is observed in approximately 15% cases (5, 6). These mutations impair the ability to repair DNA double-strand breaks (DSB) via homologous recombination (HR). The Cancer Genome Atlas consortium suggested that HR defects may be present in approximately 50% HGSC through a variety of additional mechanisms, including somatic *BRCA1/2* mutation and epigenetic loss of BRCA1 expression (4). Another key development has been the finding that HGSC may arise in the fimbriae of the fallopian tube, rather than the ovarian surface epithelium (OSE; ref. 7). Early serous tubal intra-epithelial carcinoma (STIC) lesions in the tubal fimbriae are observed in up to 10% of women with germline *BRCA1/2* mutations undergoing prophylactic salpingo-oophorectomy (8). Although a tubal origin of HGSC is widely accepted (9), STIC lesions are only seen in around half of HGSC cases (10). Recent data from mouse models (11, 12) and clinical HGSC samples (13) suggest that the ovary itself may still be crucial in the pathogenesis of HGSC, and it is possible that there could be more than one origin of this tumor.

The absence of reliable murine models has been a major impediment in HGSC research (14). This is particularly important for investigation of the immune microenvironment. The presence of tumor-infiltrating CD8 T lymphocytes (TIL) and tertiary intraepithelial lymphoid aggregates are both associated with improved prognosis in HGSC (15, 16), whereas intratumoral immunosuppressive myeloid and lymphoid cells (17, 18) are associated with poor prognosis. However, it is unclear whether or how specific genomic events in HGSC influence the immune microenvironment.

The ID8 model, first described in 2000 (19), remains the only transplantable murine model of ovarian cancer routinely

[1]Wolfson Wohl Cancer Research Centre, Institute of Cancer Sciences, University of Glasgow, Glasgow, United Kingdom. [2]Centre for Cancer and Inflammation, Barts Cancer Institute, Queen Mary University of London, London, United Kingdom. [3]Cancer Research UK Beatson Institute, Glasgow, United Kingdom. [4]Centre for Molecular Oncology, Barts Cancer Institute, Queen Mary University of London, London, United Kingdom. [5]Department of Pathology, Institute of Cancer Sciences, University of Glasgow, Glasgow, United Kingdom.

Note: Supplementary data for this article are available at Cancer Research Online (http://cancerres.aacrjournals.org/).

Corresponding Author: Iain A. McNeish, University of Glasgow, Wolfson Wohl Cancer Research Centre, Garscube Estate, Glasgow G61 1QH, United Kingdom. Phone: 44-141-330-3968; Fax: 44-141-330-4127; E-mail: iain.mcneish@glasgow.ac.uk

doi: 10.1158/0008-5472.CAN-16-1272

available. Whole ovaries from C57Bl/6 mice were trypsin-digested, and the dissociated cells passaged *in vitro*, initially in the presence of EGF. After approximately 20 passages, cells lost contact inhibition, and ten separate clones were derived, of which ID8 is the most widely used. Following intraperitoneal injection of ID8 in syngeneic mice, diffuse peritoneal carcinomatosis, with blood-stained ascites, develops in approximately 110 days (19). Over 100 publications have utilized the ID8 model, but none has characterized it in light of current understanding of human ovarian cancer biology.

Here, we show that parental ID8 lacks mutations in *Trp53*, *Brca1*, and *Brca2*, and demonstrates HR competence in functional assays. We have used CRISPR/Cas9 gene editing technology to generate single (*Trp53*) and double (*Trp53;Brca2*) knockout derivatives of ID8 and evaluated their utility as a model of human HGSC. In particular, we show that loss of individual genes results in significant alterations in immune cell infiltration into the tumor microenvironment.

Materials and Methods

Cell culture

ID8 cells, obtained from Dr. Katherine Roby (University of Kansas Medical Center, Kansas City, KS), were cultured in DMEM supplemented with 4% fetal calf serum, 100 μg/mL penicillin, 100 μg/mL streptomycin, and ITS (5 μg/mL insulin, 5 μg/mL transferrin, and 5 ng/mL sodium selenite). As ID8 was obtained directly from their original source, separate short tandem repeat validation was not performed. For cytotoxicity assays, cells were plated onto 24 well plates (3×10^3 cells/well) in triplicate. Survival was assessed by MTT assay (Nutlin-3) or sulphorhodamine B assay (rucaparib) after 72 hours.

Next-generation sequencing

Whole-exome sequencing and analysis were performed by Beckman Coulter Genomics. Full details are given in Supplementary Methods. Summary results are presented in Supplementary Tables S1 to S3. Primary sequencing data (BAM and VCF files) are available in the ArrayExpress database (http://www.ebi.ac.uk/arrayexpress) under accession number E-MTAB-4663.

Sanger sequencing

Confirmatory Sanger sequencing of exons 2 to 9 of *Trp53* was also performed on genomic DNA extracted from 10^7 parental ID8 cells in log-growth phase as well as from five separate ID8-microdissected tumors extracted from female C57Bl/6 mice after 110 days of intraperitoneal growth.

CRISPR/Cas9 and selection

Two open-access software programs, CHOPCHOP (https://chopchop.rc.fas.harvard.edu/) and CRISPR design (http://crispr.mit.edu/), were used to design guide RNAs (gRNA) targeted to *Trp53* exon 5 and *Brca2* exon 3. Three guides were designed per gene. Annealed oligonucleotides were ligated into BbsI-linearized pSpCas9(BB)-2A-Puro [PX459 (20), gifts from Feng Zhang via Addgene]. Version 1 (Addgene # 48139) was employed for *Trp53* deletion and version 2.0 (Addgene # 62988) for *Brca2*. All plasmids were sequenced to confirm successful ligation.

ID8 cells (4×10^5) were plated overnight in antibiotic-free medium, and transfected with 4 μg PX459 using Lipofectamine 2000, selected under puromycin (2.5 μg/mL) for 48 hours and plated onto 96-well plates (10 cells/mL). Single-cell colonies were expanded for DNA extraction, protein extraction, and cryopreservation.

PCR primers spanning potential sites of deletion were designed (*Trp53*: F 5′-cttccctcacattcctttcttg-3′; R 5′-gctgttaaagtagaccctgggc-3′, *Brca2*: F 5′-catggagggagtcacctttg-3′, R 5′-gctctggctgtctcgaactt-3′). Clones with large PCR deletions were selected for subsequent analysis. Remaining clones were screened using the Surveyor Nuclease Assay (Integrated DNA Technology). Mutations were confirmed by Sanger sequencing. All sequence alignment was performed using MAFFT version 7 (http://mafft.cbrc.jp/).

Immunoblot and cytokine array

Note that 15 μg of total protein was electrophoresed at 140 V for 1 hour, transferred onto nitrocellulose, and blocked in 5% nonfat milk. Antibodies used were as follows: p53 (CM5, Novacastra and Ab26, Abcam) and β-actin (Sigma; A1978). Membranes were exposed on a Chemi-doc MP (Biorad) with ECL (β actin) and ECL prime (p53). For array experiments, 5 mL supernatant was collected from 10^6 cells plated for 16 hours on a 10-cm plate, and centrifuged (2,000 rpm for 5 minutes). Mouse Cytokine Antibody Array C1 (C-series) was blotted according to the manufacturer's instructions (RayBiotech, Inc.).

Quantitative reverse transcriptase PCR

RNA was extracted from 3×10^5 cells in log-growth phase, and 2 μg was reverse transcribed (Applied Biosystems High Capacity Reverse Transcription Kit). cDNA (50 ng) was amplified using 10x iTaq qRT-PCR master mix (Biorad), 20X primer probe mix in a total of 20 μL under the following cycle parameters: 2 minutes: 50°C, 10 minutes: 95°C, 40X (15 seconds: 95°C; 1 minute: 60°C). All qRT-PCR primers were purchased from Applied Biosystems and *Trp53* custom made from Sigma Aldrich: F 5′-catcacctcactg-catggac-3′, R 5′-cttcacttgggccttcaaaa-3′, probe 5′-ccccaggatgttgag-gagt-3′. Values were normalized to Rpl-34.

γH2AX/Rad51 assay

Cells were seeded on coverslips and treated with rucaparib (10 μmol/L for 24 hours) or irradiated (10 Gy), permeabilized with 0.2% Triton (Sigma) in PBS for 1 minute, then fixed in 3% paraformaldehyde, and 2% sucrose for 10 minutes. Cells were stained with anti-γH2AX antibody (Millipore) and costained with anti-Rad51 (Santa Cruz Biotechnology) antibody for 45 minutes at 37°C. Cells were costained with DAPI. Coverslips were mounted on slides and images captured using a Zeiss 710 confocal microscope and foci counted using ImageJ software. Cells were deemed HR competent if the number of Rad51 foci more than doubled in the presence of DNA DSB damage (≥2-fold increase in number of γH2AX foci) as previously described (21).

In vivo experiments

All experiments were complied with the UK welfare guidelines (22) and were conducted under specific personal and project license authority. Cells (5×10^6) were inoculated intraperitoneally in 6- to 8-week-old female C57Bl/6 mice (Charles River Laboratories). Mice were monitored regularly and killed upon reaching UK Home Office limits. All decisions about animal welfare and experiment endpoints were made by one of us (D. Athineos) independently of main study investigators to prevent bias. Ascites was collected, and all visible tumor deposits dissected out. Half of tumor material was snap frozen (dry ice) and half

fixed in neutral-buffered 4% paraformaldehyde. Sections (5 μm) from formalin-fixed paraffin-embedded tumors were stained (Dako Autostainer, Dako) and quantified as detailed in Supplementary Methods.

Ascites preparation, tumor disaggregation, and flow cytometry

Ascites was centrifuged (2,200 rpm, 10 minutes) and supernatant stored at −80°C. The cell pellet was treated with red blood cell lysis buffer (Sigma Aldrich—5 minutes, room temperature), resuspended in 10 mL PBS, recentrifuged, and stored at −80°C in FBS/10% DMSO. Solid tumor deposits in ice-cold PBS/protease inhibitor solution were dissected into pieces less than 1 mm diameter using a scalpel and digested at 37°C for 30 minutes (0.012% w/v collagenase type XI, 0.012% w/v dispase, 0.25% Trypsin in 0.1% BSA in RPMI.) Note that 10 mL of 0.1% BSA/RPMI was added, and the tubes shaken vigorously followed by 100-μm filtration. Cells were centrifuged for 5 minutes at 1,500 rpm, resuspended in PBS containing 5% FBS, and then counted. Flow cytometry and gating strategies are presented in Supplementary Methods.

Results

Characterization of parental ID8 *in vitro* and *in vivo*

To assess the genomic landscape of ID8, we undertook whole-exome sequencing, covering approximately 194,000 exons at a mean depth of 400× with 90% exons sequenced >50×. Approximately 6,000 variants were identified, the vast majority of which were nonfunctional. Functional alterations (nonsynonymous coding, stop-gain, and frameshift) were identified in approximately 100 genes, the large majority of which were nonsynonymous coding (See Supplementary Tables S1–S3 for summary and list of all functional alterations). However, we were unable to identify any functional mutations in genes characteristic of HGSC (*Trp53*, *Brca1*, *Brca2*, *Nf1*, *Rb1*), and the absence of *Trp53* mutations was confirmed by Sanger sequencing (data not shown). In addition, mutations typical of clear cell (*Arid1A*, *Pik3ca*), low-grade serous (*Braf*), endometrioid (*Ctnnb1*), and mucinous (*Kras*) carcinomas were also notably absent. We did identify a mutation in *Adamts3* (c.1089C>T; pV199I)—a recent analysis of The Cancer Genome Atlas (TCGA) data identified that mutations in *ADAMTS* genes were associated with platinum sensitivity as well as improved progression-free and overall survival in HGSC (23). In addition, mutation in *Gabra6* (c.347T>G; pE22D) was identified. *GABRA6* was one of the genes mutated at statistically significant frequency in TCGA analysis—however, transcription was absent in all TCGA tumors, suggesting that *GABRA6* mutation is of minimal clinical relevance (4).

Given the centrality of *TP53* mutations in HGSC, we also assessed p53 function in ID8. There was a robust increase in p53 protein following treatment with cisplatin and the MDM2 inhibitor Nutlin-3 (Fig. 1A), with marked increases in *Cdkn1A* (p21) transcription within 4 hours of cisplatin treatment (Fig. 1B), indicating that p53 remains transcriptionally active. Sanger sequencing of intraperitoneal ID8 tumors showed no *Trp53* mutation in any tumor, including common hotspot mutations sites (R172, Y217, R245, R270—Fig. 1C), whereas immunohistochemistry (IHC) confirmed a wild-type pattern of p53 expression (Fig. 1D). IHC examination of typical HGSC markers indicated that tumors were strongly and diffusely positive for WT1, but negative for Pax8 (Fig. 1D).

The whole-exome sequencing data identified no functional abnormalities in *Brca1*, *Brca2*, or other HR genes. We confirmed that parental ID8 cells were able to form Rad51 foci in response to DNA DSB damage induced by irradiation as well as the PARP inhibitor rucaparib (Fig. 1E), and fulfilled the criteria of competent HR as previously described (21). Together, these data suggest that parental ID8 is poorly representative of human HGSC.

CRISPR/Cas9-mediated *Trp53* gene editing

Three separate gRNA constructs targeted to exon 5 of *Trp53* (Fig. 2A) were cloned into the PX459 plasmid. Following transfection and screening (Fig. 2B and C), clones were derived from all three guides (F3—guide G; A2—guide K; C7 and M20—guide R), all of which contained bi-allelic deletions in *Trp53* exon 5 (Supplementary Fig. S1), ranging from 4 bp (clone M20) to 280 bp (clone A2). All four null clones showed absent basal p53 expression by immunoblot (Fig. 2D), with significantly reduced basal transcription of *Trp53* (Fig. 2E), *Cdkn1a*, and *Bax* (Fig. 2F). There was also no increase in p53 expression following treatment with cisplatin or Nutlin-3 (Fig. 2G), nor an increase in *Cdkn1a* transcription following cisplatin (Fig. 2H). Finally, there was a significant reduction in cell death induced by Nutlin-3 in all four clones compared with parental ID8 (Fig. 2I). These results collectively indicate that all four $Trp53^{-/-}$ clones are functionally p53 deficient. We also isolated control clones that had been exposed to CRISPR plasmids (both empty PX459 and PX459 encoding *Trp53* gRNA) but did not contain any *Trp53* mutation on sequencing. These cells retained p53 transcriptional activity that was indistinguishable from parental ID8 (Supplementary Fig. S2).

We then assessed intraperitoneal growth of the $Trp53^{-/-}$ clones. Following intraperitoneal injection into female C57Bl/6 mice, there was a highly significant reduction in time to reach predefined humane endpoints with all four clones. Median survival time ranged from 42 to 57 days (Fig. 3A), compared with 101 days for mice bearing either parental ID8 or CRISPR control cells ($P < 0.0001$ for all clones compared with both parental ID8 and CRISPR controls). There was no difference in volume of ascites between parental ID8, CRISPR control, or $Trp53^{-/-}$ tumors (Fig. 3B). Macroscopically, the patterns of growth and spread within the peritoneal cavity were similar, although there was some evidence of increased numbers of miliary deposits on the peritoneum and diaphragm in $Trp53^{-/-}$ tumors (Fig. 3C). By IHC, we confirmed the absence of p53 expression in $Trp53^{-/-}$ tumors (Fig. 3D). $Trp53^{-/-}$ tumors retained strong positivity for WT1, but remained negative for Pax8 (Fig. 3E). We also observed significant increases in Ki67 expression in $Trp53^{-/-}$ tumors (Fig. 3F), consistent with their more rapid intraperitoneal growth.

Generation of double $Trp53^{-/-}$;$Brca2^{-/-}$ mutants

We next targeted exon 3 of *Brca2*, which encodes the PALB2 binding domain (Fig. 4A). Using the F3 $Trp53^{-/-}$ clone, we generated three separate double $Trp53^{-/-}$;$Brca2^{-/-}$ clones (1.4, 2.14, and 3.15), each derived from a different guide, and each with distinct deletions (Supplementary Fig. S3). All three $Trp53^{-/-}$;$Brca2^{-/-}$ clones fulfilled the criteria for defective HR (Fig. 4B; ref. 21) and lost the ability to form Rad51 foci in response to irradiation (Fig. 4C; Supplementary Fig. S4). In addition, all clones were significantly more sensitive to PARP inhibitor–mediated cytotoxicity (Fig. 4D). By contrast, control cells ($Trp53^{-/-}$ cells exposed to PX459 encoding *Brca2* gRNA but with no *Brca2* deletion) had the same sensitivity to rucaparib as parental ID8

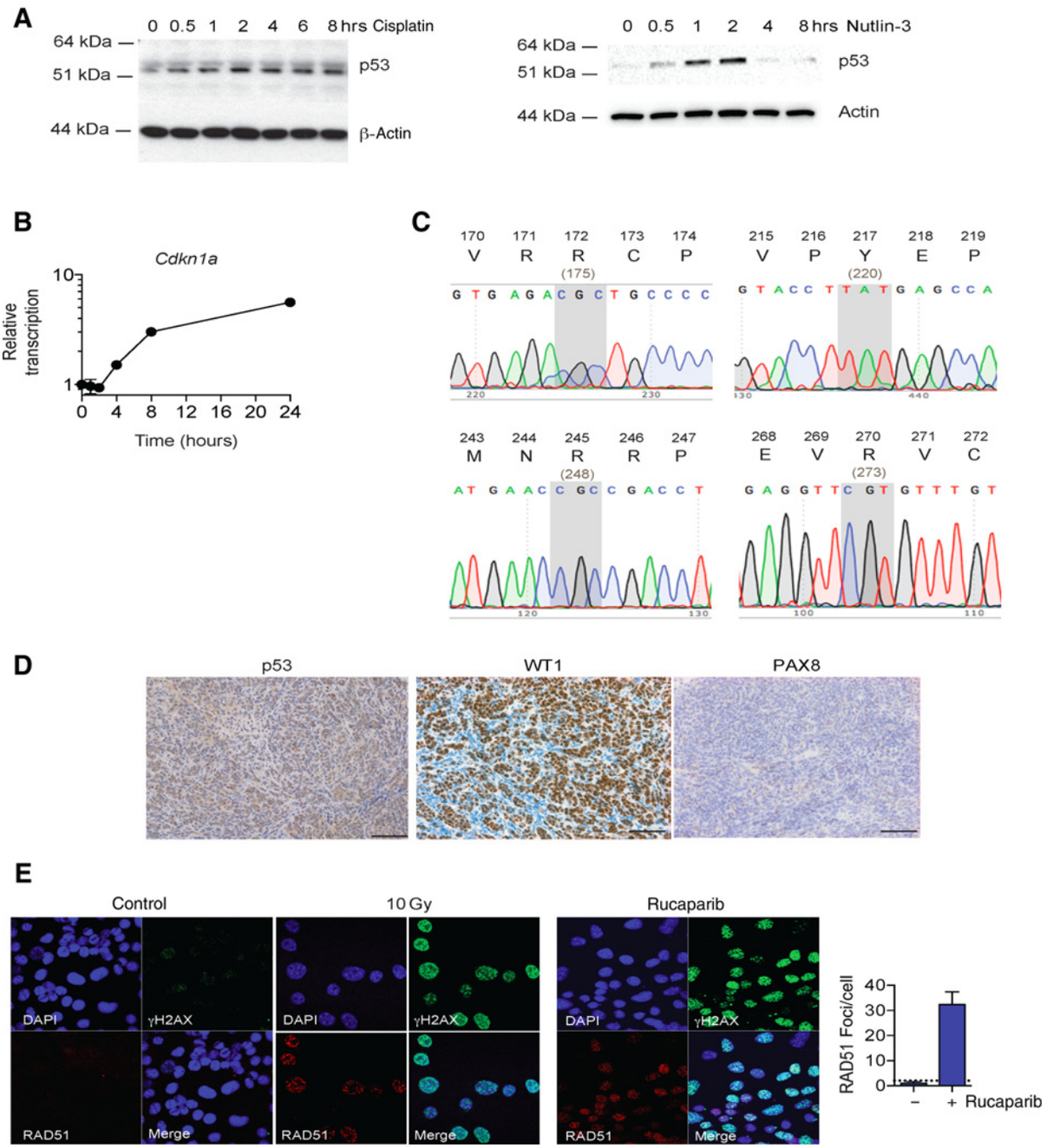

Figure 1.

ID8 retains wild-type p53 function and demonstrates competent homologous recombination. **A,** expression of p53 was assessed in ID8 cells following treatment for up to 8 hours with 10 μmol/L cisplatin (left) or 10 μmol/L Nutlin-3 (right). **B,** transcription of p53 target *Cdkn1a* in ID8 cells following treatment for up to 8 hours with 10 μmol/L cisplatin was assessed by quantitative reverse-transcriptase PCR, normalized to *Rpl34*. Data represent mean ± SD ($n = 3$) plotted relative to untreated cells ($t = 0$ hours). **C,** representative chromatograms of Sanger sequencing of p53 from parental ID8 tumors harvested after 110 days intraperitoneal growth in female C57Bl/6 mice, demonstrating no mutations at critical hotspot mutations sites at residues 172, 217, 245, and 270—the equivalent human codons are shown in parentheses below. **D,** ID8 tumors, fixed in 4% neutral-buffered formalin, were stained for p53, WT1, and PAX8. Bars, 100 μm. **E,** ID8 cells were irradiated (10 Gy) or treated with rucaparib (10 μmol/L for 24 hours), fixed and stained for γH2AX and RAD51, and counterstained with DAPI. RAD51 foci were counted in up to 30 untreated and rucaparib-treated cells. Bars, mean (± SD) RAD51 foci per cell; dotted line, two-fold increase in RAD51 foci/cell relative to untreated cells, suggestive of functional homologous recombination (21).

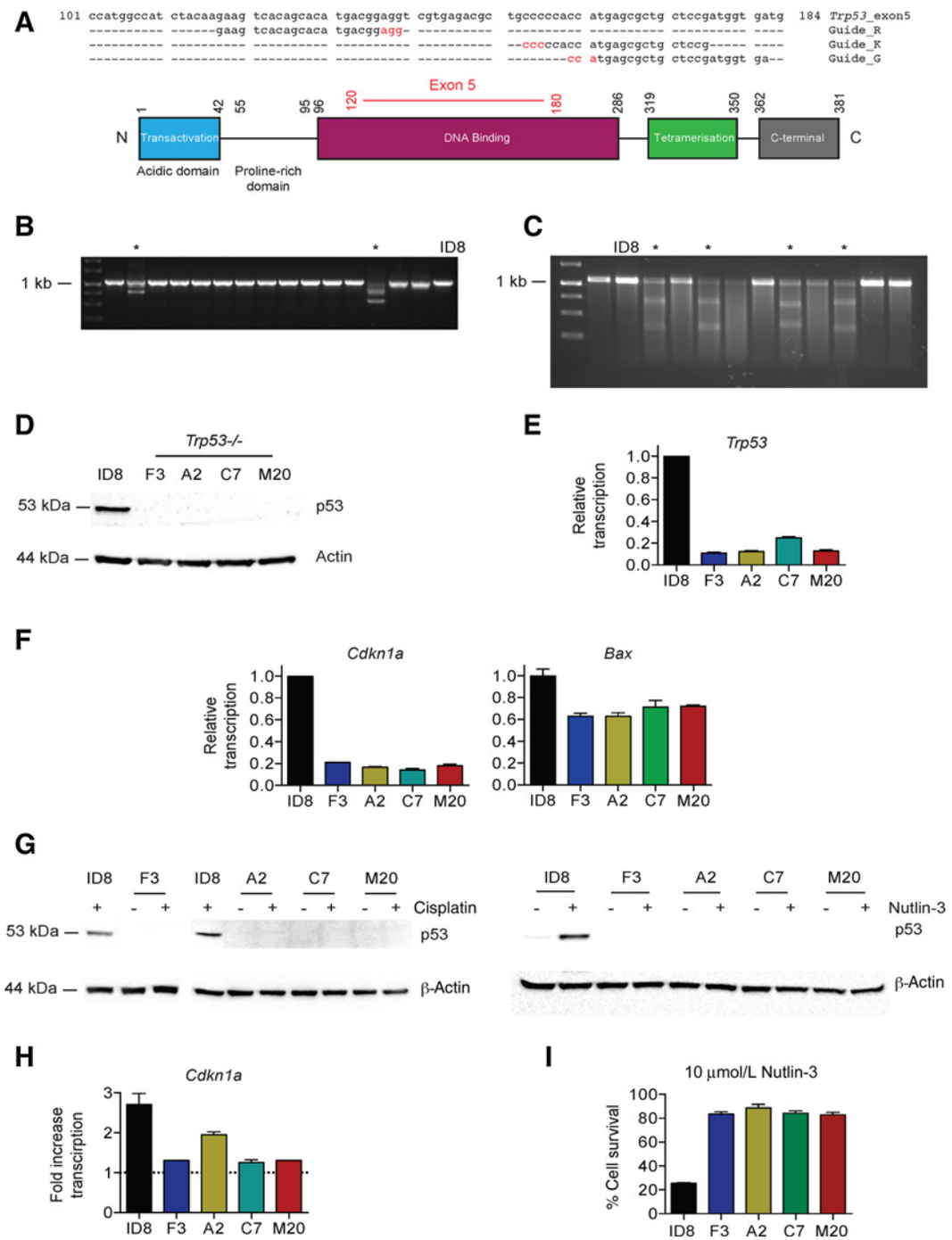

Figure 2.

Generation and evaluation of *Trp53*$^{-/-}$ ID8 cells using CRISPR/Cas9. **A,** design of three gRNA sequences, targeted to exon 5 of *Trp53* (top). Nucleotides in red represent PAM sequences. Schematic representation of p53 protein (bottom). Numbers represent amino acid positions. Amino acids encoded by exon 5 are marked in red. **B,** representative PCR of 1 kb region spanning *Trp53* exon 5 from genomic DNA extracted from ID8 and 15 single cell clones transfected with PX459 expressing gRNA K. *, clones with demonstrable deletions. **C,** representative Surveyor Nuclease Assay performed on ID8 and 11 single cell clones transfected with PX459 expressing *Trp53* gRNA K as described in Material and Methods. *, clones with mismatch suggestive of nucleotide deletion. **D,** expression of p53 was assessed in parental ID8 and four *Trp53*$^{-/-}$ clones by immunoblot. **E,** transcription of *Trp53* was assessed in parental ID8 and four *Trp53*$^{-/-}$ clones by quantitative reverse-transcriptase PCR, normalized to *Rpl34*. Bars, mean ± SD ($n = 3$) plotted relative to parental ID8. **F,** transcription of p53 target genes *Cdkn1a* and *Bax* was assessed in parental ID8 and *Trp53*$^{-/-}$ clones by quantitative reverse-transcriptase PCR, normalized to *Rpl34*. Bars, mean ± SD ($n = 3$) plotted relative to parental ID8. **G,** expression of p53 in ID8 and *Trp53*$^{-/-}$ clones before and after cisplatin (10 μmol/L, 8 hours, left) and Nutlin-3 (10 μmol/L, 2 hours, right). **H,** fold increase in *Cdkn1a* transcription in ID8 and *Trp53*$^{-/-}$ clones following cisplatin treatment (10 μmol/L, 8 hours). Bars, mean ± SD ($n = 3$); dotted line, baseline transcription in each cell population. **I,** ID8 and *Trp53*$^{-/-}$ clones were treated with 10 μmol/L Nutlin-3 and cell survival assessed by MTT after 72 hours. Bars, cell survival (mean ± SD, $n = 3$) relative to untreated cells.

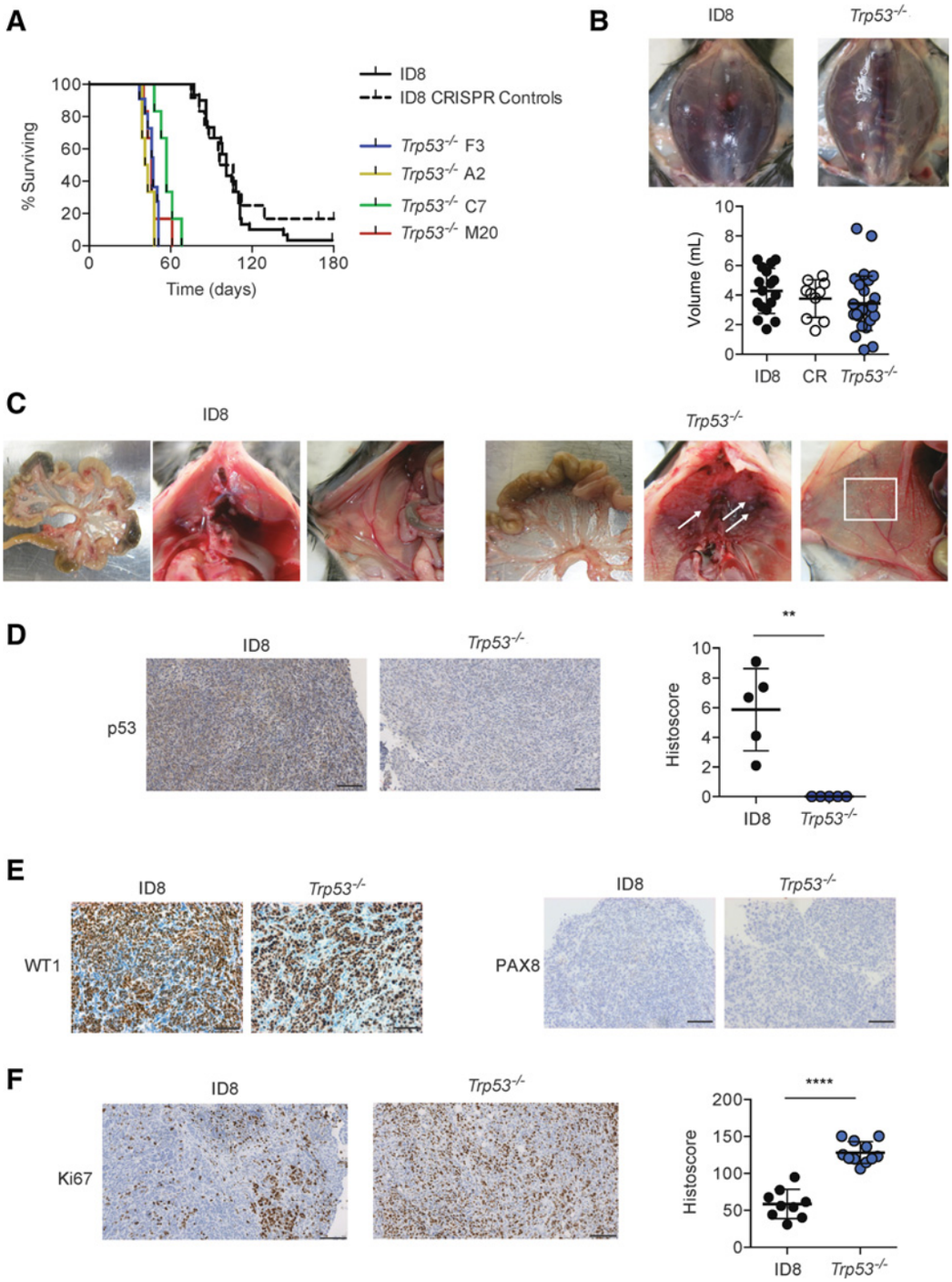

Figure 3.

Loss of p53 increases rate of intraperitoneal growth of ID8 tumors. Cells (5×10^6) were injected intraperitoneally into female C57Bl/6 mice in groups of six. Mice were killed when they reached humane endpoints. Ascites was taken from all mice and measured. Each point on histoscore plot represents mean score for multiple deposits (median 5; range, 1–17) per animal normalized to tumor area. **A,** loss of p53 significantly increases rate of intraperitoneal growth ($P < 0.0001$ for all *Trp53*$^{-/-}$ clones compared with both parental ID8 and CRISPR control cells). Data from four ID8 parental groups (total $n = 24$) and two groups each of CRISPR control and *Trp53*$^{-/-}$ F3 (total $n = 12$) are plotted. **B,** loss of p53 does not alter volume of ascites at humane endpoint. **C,** loss of p53 increases number of tumor deposits on peritoneal (white box) and subdiaphragmatic (arrows) surfaces. Representative images from at least three mice per genotype. **D,** loss of p53 expression was confirmed by quantitative IHC in *Trp53*$^{-/-}$ tumors. **, $P < 0.01$. **E,** no change in WT1 and PAX8 expression following p53 loss. **F,** loss of p53 expression significantly increases intraperitoneal tumor proliferation, as measured by Ki67 staining. ****, $P < 0.0001$.

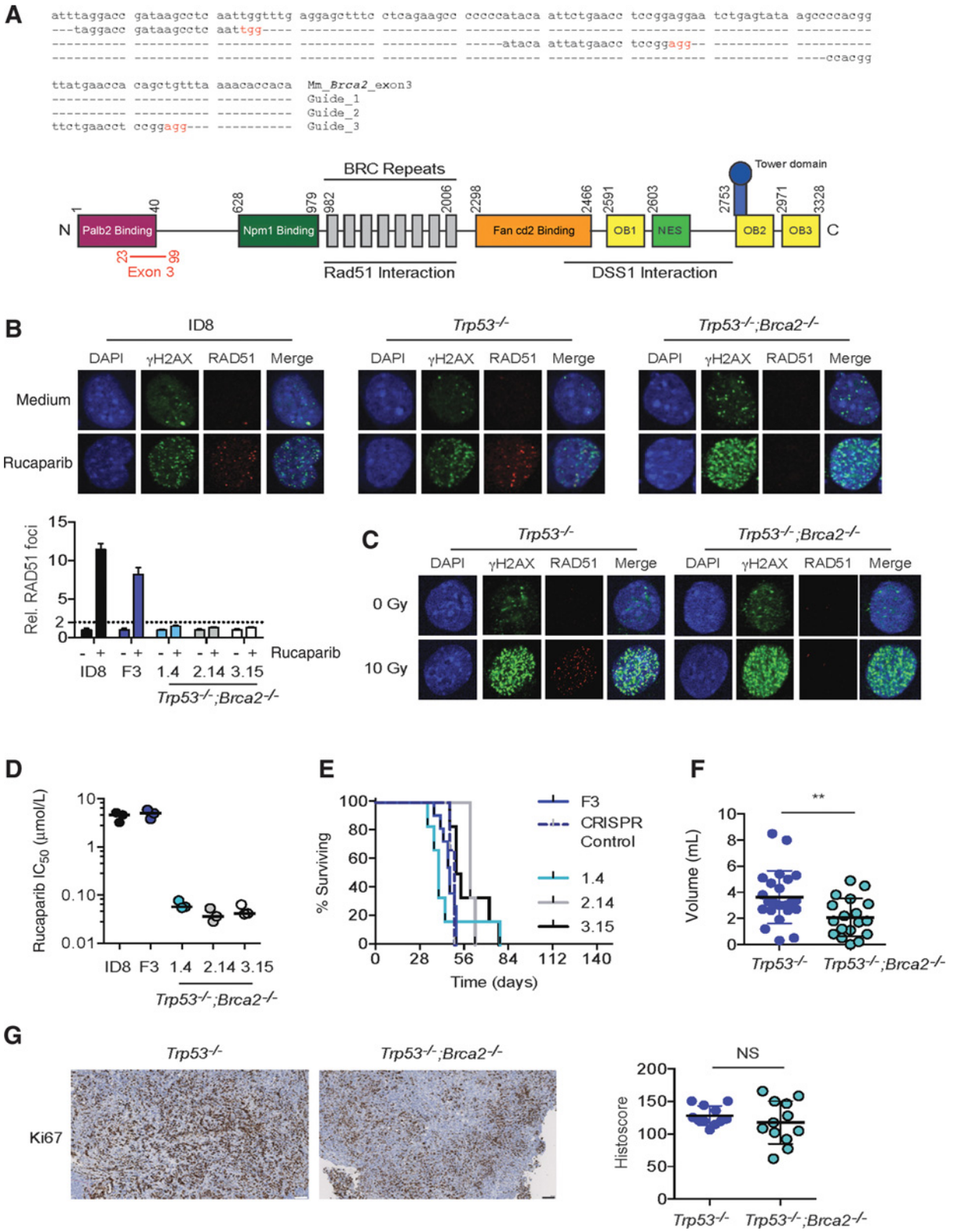
A
atttaggacc gataagcctc aattggtttg aggagctttc ctcagaagcc ccccctataca attctgaacc tccggaggaa tctgagtata agccccacgg
---taggacc gataagcctc aattgg---- ---------- ---------- ---------- ---------- ---------- ---------- ----------
---------- ---------- ---------- ---------- ---------- -----ataca attatgaacc tccggagg-- ---------- ----------
---------- ---------- ---------- ---------- ---------- ---------- ---------- ---------- ---------- ----ccacgg
ttatgaacca cagctgttta aaacaccaca Mm_Brca2_exon3
---------- ---------- ---------- Guide_1
---------- ---------- ---------- Guide_2
ttctgaacct ccggagg--- ---------- Guide_3
BRC Repeats
Tower domain
N
Palb2 Binding
Npm1 Binding
Fan cd2 Binding
OB1
NES
OB2
OB3
C
Exon 3
Rad51 Interaction
DSS1 Interaction
B
ID8
Trp53-/-
Trp53-/-;Brca2-/-
DAPI
γH2AX
RAD51
Merge
Medium
Rucaparib
Rel. RAD51 foci
Rucaparib
ID8 F3 1.4 2.14 3.15
Trp53-/-;Brca2-/-
C
0 Gy
10 Gy
D
Rucaparib IC50 (μmol/L)
E
% Surviving
Time (days)
F3
CRISPR Control
1.4
2.14
3.15
F
Volume (mL)
**
G
Ki67
NS
Histoscore

and F3 *Trp53*$^{-/-}$, and were HR competent by Rad51 assay (data not shown).

We also assessed intraperitoneal growth of *Trp53*$^{-/-}$;*Brca2*$^{-/-}$ clones. When analyzed individually, there was no difference in mouse survival between *Trp53*$^{-/-}$ F3 tumors and any of the double null tumors (Fig. 4E). However, when analyzed collectively, there was a small, but significant, increase in survival: mice bearing *Trp53*$^{-/-}$;*Brca2*$^{-/-}$ tumors survived 10 days longer than *Trp53*$^{-/-}$ F3 tumors (57 vs. 47 days; $P < 0.01$; Supplementary Fig. S5). In addition, mice had significantly lower ascites volumes than either parental or *Trp53*$^{-/-}$ tumors (Fig. 4F). There were large diaphragmatic and peritoneal deposits, and ascites was consistently less hemorrhagic (Supplementary Fig. S6). Ki67 histoscores were significantly higher than ID8 parental tumors (not shown) but not significantly different to those seen in *Trp53*$^{-/-}$ (Fig. 4G).

Tumor microenvironment

To investigate the utility of our new ID8 derivatives to study the relationship between specific mutations within malignant cells and the tumor microenvironment, we first stained tumors for the presence of T lymphocytes (both CD3 and CD8) and macrophages (F4/80). Intraepithelial CD3$^+$ and CD8$^+$ cells were both generally sparse, with no significant differences between any of the tumor genotypes (Fig. 5A and B). However, we observed the presence of lymphoid aggregates within *Trp53*$^{-/-}$;*Brca2*$^{-/-}$ tumors that were absent from both parental ID8 and *Trp53*$^{-/-}$tumors (Fig. 5C; Supplementary Figs. S7 and S8). These aggregates were composed predominantly of CD3$^+$ cells, although CD8$^+$ populations were visible at the periphery (Supplementary Fig. S9). We also observed striking and significant increases in macrophage infiltration in *Trp53*$^{-/-}$ tumors (Fig. 5D; Supplementary Fig. S10). Macrophage infiltration was more variable in *Trp53*$^{-/-}$;*Brca2*$^{-/-}$ tumors—median histoscore was greater than in ID8 parental tumors but lower than in *Trp53*$^{-/-}$ tumors, although neither difference was statistically significant (Fig. 5D).

We next investigated the specific role of p53 loss upon myeloid populations. Immunoblot array showed marked increases in the monocyte chemoattractant CCL2, and, to a lesser extent, CCL5 and sTNFR1 in conditioned medium from *Trp53*$^{-/-}$ cells (Fig. 6A; Supplementary Fig. S11). Immunophenotyping of disaggregated solid tumor deposits (Fig. 6B; Supplementary Fig. S12) and ascites (Fig. 6C; Supplementary Fig. S12) showed significant increases in CD11b$^+$ populations in *Trp53*$^{-/-}$ tumors compared with *Trp53* wild-type. Monocytic myeloid-derived suppressor cells (defined as CD11b$^+$Ly6C$^+$Ly6G$^-$) were the predominant myeloid population in both tumor and ascites compared with polymorphonuclear (PMN) MDSC populations (CD11b$^+$Ly6C$^+$Ly6G$^+$). Consistent with IHC, we found significantly more F4/80-positive cells within *Trp53*$^{-/-}$ ascites, although the proportions of iNOS$^+$ and CD206$^+$ cells did not alter significantly between the two genotypes (Fig. 6D; Supplementary Figs. S13 and S14).

Discussion

Here, we show that ID8, a widely used murine model of ovarian carcinoma, is poorly representative of HGSC, with a conspicuous absence of mutations in genes associated with the human disease, and evidence of functional p53 activity. The overall mutational burden in ID8 is low (functional variants in only 100 genes in 49 MB of sequenced DNA), which concurs with very recent data from ID8-G7, a subline of ID8 that has been passaged *in vivo* (24). We did not observe activating mutations in common oncogenes (e.g., *Kras, Nras, Myc, Egfr, Pik3ca*) that may drive carcinogenesis in parental ID8 cells, but we have not undertaken copy-number analyses, and thus cannot exclude the presence of an oncogenic amplification.

Using CRISPR/Cas9 gene editing, we generated sublines of ID8 bearing loss-of-function deletions in *Trp53* and *Brca2*, and demonstrate that these alter tumor growth in the peritoneal cavity. In preliminary experiments, we also show that single-gene mutations can alter the tumor microenvironment, with a significant increase in immunosuppressive myeloid populations within tumor and ascites upon loss of p53 expression, as well as the appearance of intraepithelial lymphoid aggregates in tumors lacking both p53 and Brca2.

Genetically engineered mouse models of HGSC have been difficult to generate (25). Recently, two HGSC models were described: the Drapkin lab utilized the Pax8 promoter to drive Cre-mediated recombination of *Trp53* and *Pten* with *Brca1* or *Brca2* in mouse fallopian tube secretory epithelium. This resulted in development of STIC lesions, and subsequent invasive tumors in the ovary and peritoneal cavity within 20 weeks (26). By morphology and IHC, the tumors resembled human HGSC, but no ascites was observed, and all *Pten*$^{-/-}$ mice developed endometrial lesions (hyperplasia, dysplasia, or carcinoma). In addition, no transplantable cell lines have been described from these mice. A second fallopian tube model has been described, with SV40 large T antigen under the control of the *Ovgp-1* promoter (27, 28). Again, STIC-like lesions with p53 signatures were described, as well as invasive tumors within the ovary. However, no peritoneal dissemination or ascites was seen, and, again, no lines that can be readily transplanted into nontransgenic mice have been described. Both of these models are undoubtedly of

Figure 4.

Generation and evaluation of *Trp53*$^{-/-}$;*Brca2*$^{-/-}$ ID8 cells using CRISPR/Cas9. **A,** design of three gRNA sequences, targeted to exon 3 of *Brca2* (top). Nucleotides in red represent PAM sequences. Schematic representation of Brca2 protein (bottom). Numbers represent amino acid positions. OB, oligonucleotide binding domain; NES, nuclear export signal. Amino acids encoded by exon 3 are marked in red. **B,** parental ID8, *Trp53*$^{-/-}$ cell line F3, and three *Trp53*$^{-/-}$;*Brca2*$^{-/-}$ cells were treated with rucaparib (10 μmol/L), fixed and stained for γH2AX and RAD51, and counterstained with DAPI. Representative confocal microscopy images are presented (top). RAD51 foci were counted in up to 30 untreated and rucaparib-treated cells. Bars, mean (± SD) foci per cell relative to untreated cell; dotted line, two-fold increase in foci/cell relative to untreated cells. **C,** *Trp53*$^{-/-}$ cell line F3 and *Trp53*$^{-/-}$;*Brca2*$^{-/-}$ 3.15 cells were irradiated (10 Gy), fixed and stained for γH2AX and RAD51, and counterstained with DAPI. **D,** *Trp53*$^{-/-}$;*Brca2*$^{-/-}$ cells are significantly more sensitive to PARP inhibitor–induced cytotoxicity than either parental ID8 or *Trp53*$^{-/-}$ cell line F3. Each dot represents IC_{50} value from a single experiment performed in triplicate. Bars represent median IC_{50} for three separate experiments. **E,** cells (5×10^6) were injected intraperitoneally into female C57Bl/6 mice in groups of six. Mice were killed when they reached humane endpoints. Ascites was taken from all mice and measured. F3 CRISPR control cells are *Trp53*$^{-/-}$ F3 cells exposed to PX459 encoding *Brca2* gRNA (Guide 1), but which contain no deletion in *Brca2* on sequencing. **F,** loss of Brca2 and p53 reduces volume of ascites compared with loss of p53 alone. **, $P < 0.01$. **G,** additional loss of Brca2 expression does not significantly alter intraperitoneal tumor proliferation, as measured by Ki67 staining. Bars on IHC images, 100 μm. Each dot represents mean histoscore for multiple deposits (median 5; range, 1–17) per animal, normalized to tumor area.

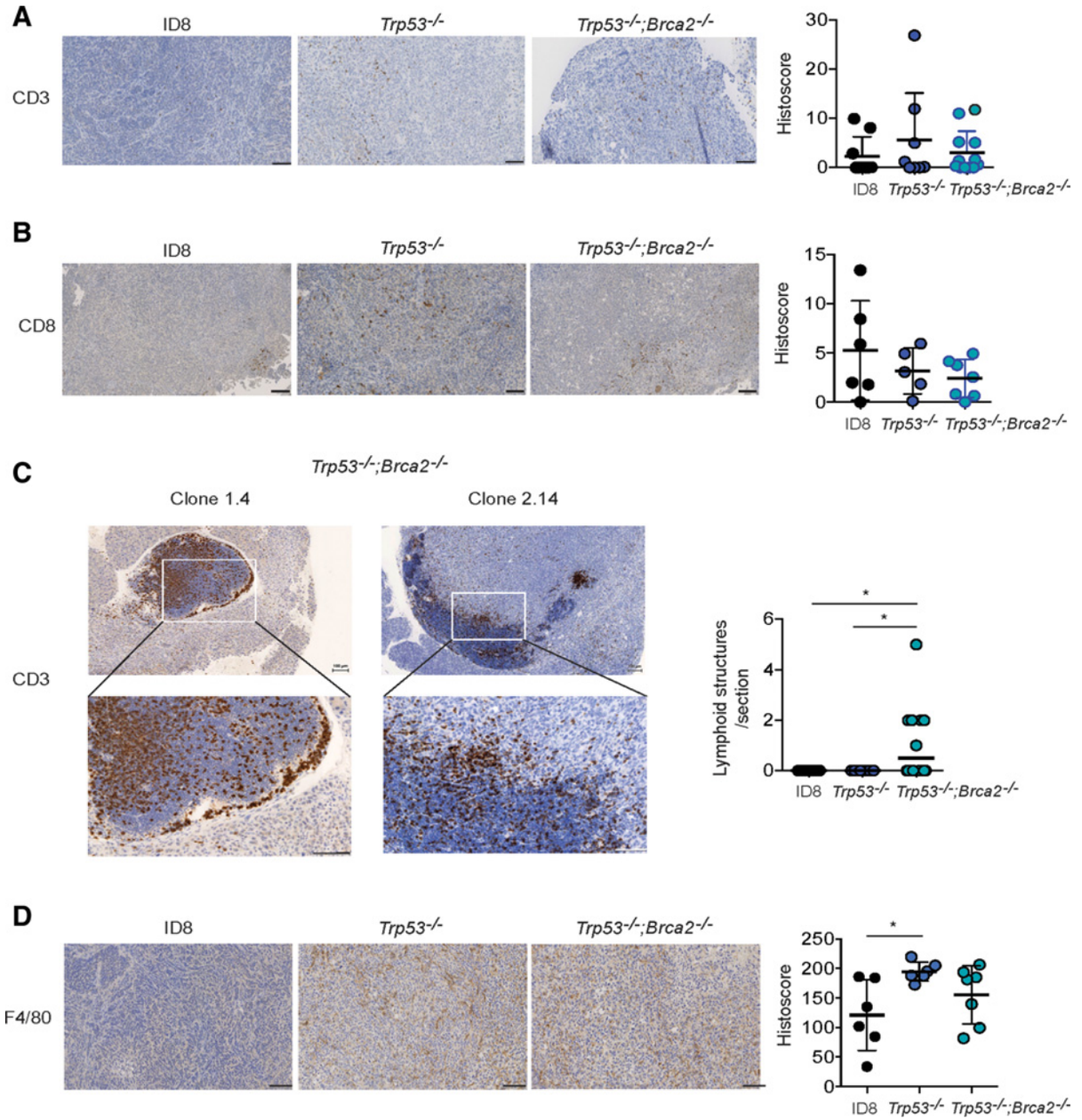

Figure 5.

Loss of p53 and Brca2 expression alters immune cell infiltration in ID8 tumors. Formalin-fixed, paraffin-embedded tumors from all three genotypes (parental ID8, *Trp53*$^{-/-}$, and *Trp53*$^{-/-}$;*Brca2*$^{-/-}$) were stained for CD3 (**A**) and CD8 (**B**). **C,** the number of intraepithelial lymphoid aggregates, defined as an area >0.1 mm^2, was counted in tumors from all three genotypes. No aggregates were identified in ID8 and *Trp53*$^{-/-}$ tumors. Bar, median. *, $P < 0.05$. **D,** tumors were also stained for F4/80. Bars, 100 μm. Intensity of expression was quantified as detailed in Materials and Methods. Each dot represents mean histoscore for multiple deposits per animal, normalized to tumor area. *, $P < 0.05$.

great importance. However, we believe that a transplantable model, based on a single genetic background (C57Bl/6), which recapitulates disseminated peritoneal disease with ascites and in which multiple genotypes can potentially be rapidly investigated in parallel, is an important adjunct to transgenic models.

One potential criticism of our models is that they arise from a single cell line. Although other murine ovarian cancer cell lines have been described (29), they derive from chimeric SV40 T-Ag animals, and thus cannot be transplanted into nontransgenic animals, which significantly reduces their utility. ID8 remains the only murine line derived from a single nontransgenic strain from which to base these models. A second potential criticism is the cell of origin of ID8 itself. In the original description of ID8 (19), whole mouse ovaries were trypsinized with the aim of

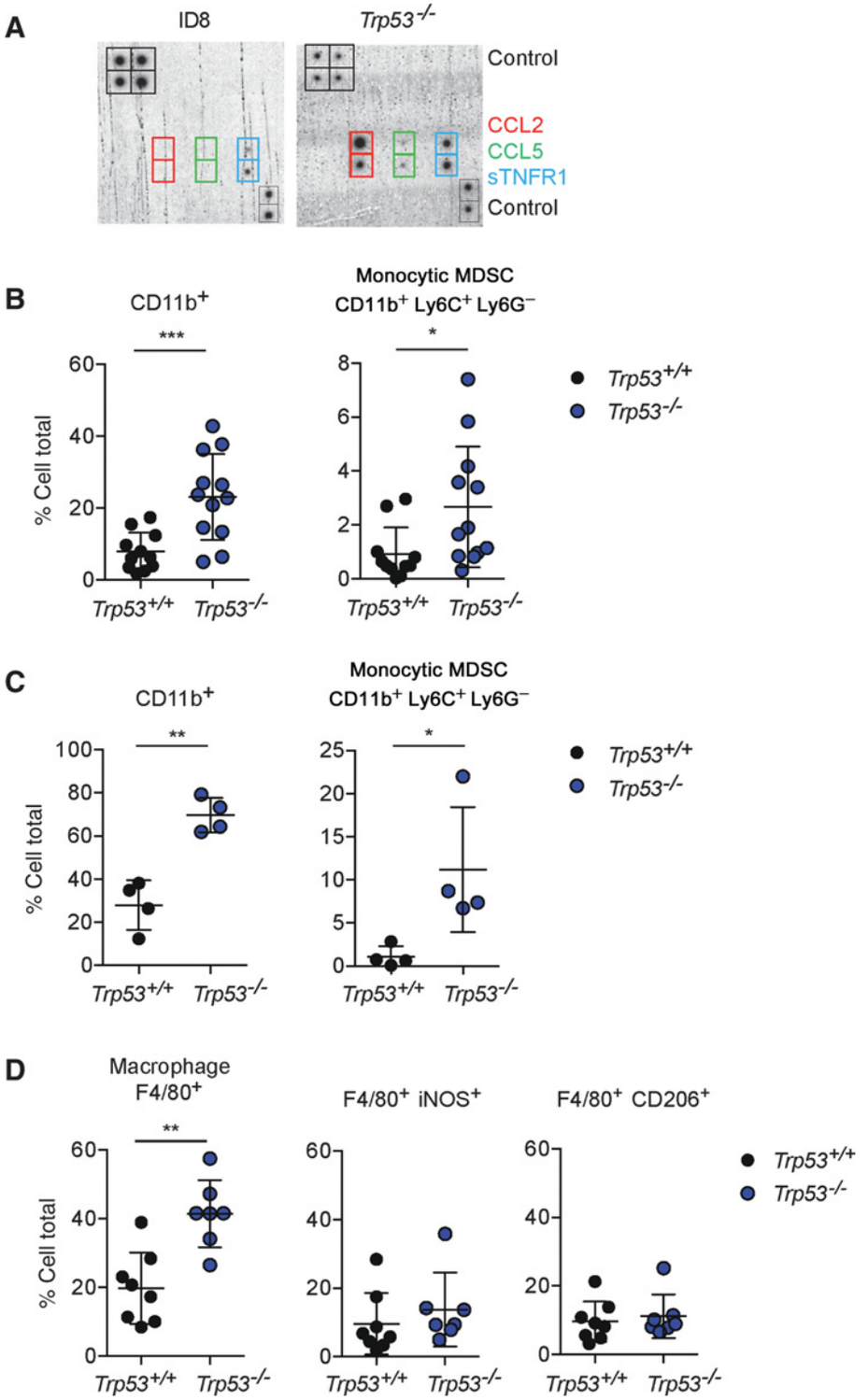

Figure 6.
Loss of p53 expression increases CCL2 expression and induces immunosuppressive myeloid cell infiltration in tumor and ascites. **A,** expression of chemokines in conditioned medium was assessed using immunoblot array. See Supplementary Fig. S9 for complete array layout. **B–D,** disaggregated whole tumor deposits (**B**) and ascites cells (**C** and **D**) were assessed by flow cytometry for CD4, CD8, CD11b, Ly6G, Ly6C, F4/80, CD206, and iNOS. Each dot represents a single tumor deposit (minimum three deposits/mouse) or ascites sample. Bars, mean ± SD. *Trp53*$^{+/+}$ populations include ID8 parental and CRISPR control cells lacking any *Trp53* mutation. *, $P < 0.05$; **, $P < 0.01$; ***, $P < 0.001$.

removing the OSE layer, but the exact cell of origin of ID8 is unclear. Although the fallopian tube is undoubtedly the originating site of many HGSC, a potential ovarian origin is possible for a subset of these tumors (13). In addition, data from the Drapkin lab model indicated that oophorectomy reduced peritoneal dissemination, suggesting that the ovary plays a role in promoting metastatic spread of fallopian tube lesions (26). Thus, an OSE origin of ID8 does not preclude the applicability of our new cells as a model of HGSC, and our tumors do express some typical HGSC markers (e.g., WT1). However, the absence of Pax8

staining strongly suggests that ID8 is not of fallopian tube secretory origin. PAX8 staining is used in the diagnosis of HGSC and is usually strongly positive, although this is not universal (30). Therefore, the absence of Pax8 in our ID8 models is important to note, but is not a barrier to their use in HGSC research.

Although CRISPR/Cas9 gene editing is an extremely powerful tool, off-target effects can occur (31, 32), which are difficult to quantify precisely in any given model without whole-genome sequencing. Here, we used multiple different guides and selected at least one clone per guide. In addition, we utilized appropriate negative controls (cells exposed to CRISPR plasmid transfection but that do not contain mutations in target gene). The uniform phenotypes observed in each of our models suggest strongly that any off-target effects are not significant.

Finally, we have undertaken preliminary experiments to investigate the link between tumor-specific mutations and immune composition in the microenvironment. Here, we show that loss of p53 increases CCL2 expression and induces marked increases in immunosuppressive myeloid populations both within solid tumor deposits and ascites. CCL2 is a critical chemokine for attraction of monocyte populations; wild-type p53 can suppress CCL2 expression via direct binding to the CCL2 5′UTR (33) and can reduce CCL2-induced xenograft growth (34). In *Trp53*$^{-/-}$ tumors, there appeared to be a bias toward monocytic MDSC populations, which have been characterized as more immunosuppressive than PMN MDSC in tumor-bearing mice (35). Intriguingly, we also observed aggregates of lymphoid cells in tumors lacking both p53 and Brca2. The structures contained hundreds of cells, which were predominantly CD3^{+} but CD8^{-}. Four different types of lymphoid aggregates in HGSC were recently described, the largest of which resembled activated lymph nodes (16), and which contain a variety of T- and B-cell lineages, including plasma cells. The presence of plasma cells was associated with expression of two genes, *IGJ* and *TNFRSF17*, but was independent of mutation in *BRCA1* or *BRCA2*. Our preliminary data suggest that loss of Brca2 and p53 can lead to formation of tertiary lymphoid aggregates, but further work, including gene expression analysis and further flow cytometry, will be required to elucidate this relationship. It is not clear whether these microenvironmental changes explain why loss of Brca2 and p53 function results in slower intraperitoneal growth compared with p53 loss alone. Ki67 staining suggests that there is no significant reduction in proliferation in the *Trp53*$^{-/-}$;*Brca2*$^{-/-}$ tumors, suggesting that non–cell-autonomous factors may be contributing. Certainly, in patients with HGSC, *BRCA2* mutation and the presence of intratumoral lymphocytes (15) are both associated with longer overall survival (36), although the precise mechanisms for this remain unclear.

In summary, we have used gene editing technology to generate transplantable murine ovarian cancer cell lines that recapitulate critical mutations in human HGSC. Our results suggest that our ID8 models may act as an important tool, alongside genetically engineered mouse models and primary patient material, in understanding the complexities of HGSC biology. Further mutants are under construction, and all our ID8 derivatives are freely available to other researchers.

Disclosure of Potential Conflicts of Interest

I.A. McNeish is a consultant/advisory board member for AstraZeneca and Clovis Oncology. No potential conflicts of interest were disclosed by the other authors.

Authors' Contributions

Conception and design: J. Walton, J. Blagih, D. Strathdee, K. Vousden, I.A. McNeish

Development of methodology: J. Walton, E. Leung, D. Stevenson, I.A. McNeish

Acquisition of data (provided animals, acquired and managed patients, provided facilities, etc.): J. Walton, D. Ennis, E. Leung, S. Dowson, M. Farquharson, L.A. Tookman, D. Athineos, S. Mason, K. Blyth, K. Vousden, I.A. McNeish

Analysis and interpretation of data (e.g., statistical analysis, biostatistics, computational analysis): J. Walton, J. Blagih, E. Leung, M. Farquharson, I.A. McNeish

Writing, review, and/or revision of the manuscript: J. Walton, J. Blagih, D. Ennis, E. Leung, S. Dowson, L.A. Tookman, D. Stevenson, K. Blyth, F.R. Balkwill, K. Vousden, M. Lockley, I.A. McNeish

Administrative, technical, or material support (i.e., reporting or organizing data, constructing databases): D. Ennis, S. Dowson, C. Orange

Study supervision: F.R. Balkwill, M. Lockley, I.A. McNeish

Acknowledgments

We would like to thank Emma Johnson for expert technical assistance with mouse experiments and Colin Nixon and Marion Stevenson for IHC.

Grant Support

This work was funded by the University of Glasgow and Cancer Research UK [grants C16420/A12995 (I.A. McNeish), C596/A18076 (K. Vousden), C608/A15973 (I.A. McNeish), C596/A20921 (K. Vousden), and C16420/A16354 (F. R. Balkwill)]. All animal work was performed in the Biological Services Unit facilities at the Cancer Research UK Beatson Institute (Cancer Research UK grant C596/A17196).

The costs of publication of this article were defrayed in part by the payment of page charges. This article must therefore be hereby marked *advertisement* in accordance with 18 U.S.C. Section 1734 solely to indicate this fact.

Received May 4, 2016; revised July 15, 2016; accepted August 2, 2016; published OnlineFirst August 16, 2016.

References

1. Perren TJ, Swart AM, Pfisterer J, Ledermann JA, Pujade-Lauraine E, Kristensen G, et al. A phase 3 trial of bevacizumab in ovarian cancer. N Engl J Med 2011;365:2484–96.
2. Bowtell DD, Bohm S, Ahmed AA, Aspuria PJ, Bast RCJr, Beral V, et al. Rethinking ovarian cancer II: Reducing mortality from high-grade serous ovarian cancer. Nat Rev Cancer 2015;15:668–79.
3. Ahmed AA, Etemadmoghadam D, Temple J, Lynch AG, Riad M, Sharma R, et al. Driver mutations in TP53 are ubiquitous in high grade serous carcinoma of the ovary. J Pathol 2010;221:49–56.
4. TCGA. Integrated genomic analyses of ovarian carcinoma. Nature 2011; 474:609–15.
5. Zhang S, Royer R, Li S, McLaughlin JR, Rosen B, Risch HA, et al. Frequencies of BRCA1 and BRCA2 mutations among 1,342 unselected patients with invasive ovarian cancer. Gynecol Oncol 2011;121:353–57.
6. Alsop K, Fereday S, Meldrum C, Defazio A, Emmanuel C, George J, et al. BRCA mutation frequency and patterns of treatment response in BRCA mutation-positive women with ovarian cancer: A report from the Australian Ovarian Cancer Study Group. J Clin Oncol 2012;30:2654–63.
7. Lee Y, Miron A, Drapkin R, Nucci MR, Medeiros F, Saleemuddin A, et al. A candidate precursor to serous carcinoma that originates in the distal fallopian tube. J Pathol 2007;211:26–35.
8. Medeiros F, Muto MG, Lee Y, Elvin JA, Callahan MJ, Feltmate C, et al. The tubal fimbria is a preferred site for early adenocarcinoma in women with familial ovarian cancer syndrome. Am J Surg Pathol 2006;30:230–6.
9. Singh N, Gilks CB, Hirschowitz L, Kehoe S, McNeish IA, Miller D, et al. Primary site assignment in tubo-ovarian high-grade serous carcinoma: Consensus statement on unifying practice worldwide. Gynecol Oncol 2016;141:195–8.

10. Kindelberger DW, Lee Y, Miron A, Hirsch MS, Feltmate C, Medeiros F, et al. Intraepithelial carcinoma of the fimbria and pelvic serous carcinoma: Evidence for a causal relationship. Am J Surg Pathol 2007;31: 161–9.
11. Flesken-Nikitin A, Hwang CI, Cheng CY, Michurina TV, Enikolopov G, Nikitin AY. Ovarian surface epithelium at the junction area contains a cancer-prone stem cell niche. Nature 2013;495:241–5.
12. Kim J, Coffey DM, Ma L, Matzuk MM. The ovary is an alternative site of origin for high-grade serous ovarian cancer in mice. Endocrinology 2015;156:1975–81.
13. Howitt BE, Hanamornroongruang S, Lin DI, Conner JE, Schulte S, Horowitz N, et al. Evidence for a dualistic model of high-grade serous carcinoma: BRCA mutation status, histology, and tubal intraepithelial carcinoma. Am J Surg Pathol 2015;39:287–93.
14. Vaughan S, Coward JI, Bast RCJr, Berchuck A, Berek JS, Brenton JD, et al. Rethinking ovarian cancer: Recommendations for improving outcomes. Nat Rev Cancer 2011;11:719–25.
15. Zhang L, Conejo-Garcia JR, Katsaros D, Gimotty PA, Massobrio M, Regnani G, et al. Intratumoral T cells, recurrence, and survival in epithelial ovarian cancer. N Engl J Med 2003;348:203–13.
16. Kroeger DR, Milne K, Nelson BH. Tumor infiltrating plasma cells are associated with tertiary lymphoid structures, cytolytic T cell responses, and superior prognosis in ovarian cancer. Clin Cancer Res 2016;22: 3005–15.
17. Curiel TJ, Coukos G, Zou L, Alvarez X, Cheng P, Mottram P, et al. Specific recruitment of regulatory T cells in ovarian carcinoma fosters immune privilege and predicts reduced survival. Nat Med 2004;10:942–49.
18. Kryczek I, Wei S, Zhu G, Myers L, Mottram P, Cheng P, et al. Relationship between B7-H4, regulatory T cells, and patient outcome in human ovarian carcinoma. Cancer Res 2007;67:8900–5.
19. Roby KF, Taylor CC, Sweetwood JP, Cheng Y, Pace JL, Tawfik O, et al. Development of a syngeneic mouse model for events related to ovarian cancer. Carcinogenesis 2000;21:585–91.
20. Ran FA, Hsu PD, Wright J, Agarwala V, Scott DA, Zhang F. Genome engineering using the CRISPR-Cas9 system. Nat Protoc 2013;8:2281–308.
21. Mukhopadhyay A, Elattar A, Cerbinskaite A, Wilkinson SJ, Drew Y, Kyle S, et al. Development of a functional assay for homologous recombination status in primary cultures of epithelial ovarian tumor and correlation with sensitivity to poly(ADP-ribose) polymerase inhibitors. Clin Cancer Res 2010;16:2344–51.
22. Workman P, Aboagye EO, Balkwill F, Balmain A, Bruder G, Chaplin DJ, et al. Guidelines for the welfare and use of animals in cancer research. Br J Cancer 2010;102:1555–77.
23. Liu Y, Yasukawa M, Chen K, Hu L, Broaddus RR, Ding L, et al. Association of somatic mutations of adamts genes with chemotherapy sensitivity and survival in high-grade serous ovarian carcinoma. JAMA Oncol 2015;1:486–94.
24. Martin SD, Brown SD, Wick DA, Nielsen JS, Kroeger DR, Twumasi-Boateng K, et al. Low mutation burden in ovarian cancer may limit the utility of neoantigen-targeted vaccines. PLoS One 2016;11:e0155189.
25. Clark-Knowles KV, Senterman MK, Collins O, Vanderhyden BC. Conditional inactivation of Brca1, p53 and Rb in mouse ovaries results in the development of leiomyosarcomas. PLoS ONE 2009;4:e8534.
26. Perets R, Wyant GA, Muto KW, Bijron JG, Poole BB, Chin KT, et al. Transformation of the fallopian tube secretory epithelium leads to high-grade serous ovarian cancer in brca;tp53;pten models. Cancer Cell 2013;24:751–65.
27. Miyoshi I, Takahashi K, Kon Y, Okamura T, Mototani Y, Araki Y, et al. Mouse transgenic for murine oviduct-specific glycoprotein promoter-driven simian virus 40 large T-antigen: Tumor formation and its hormonal regulation. Mol Reprod Dev 2002;63:168–76.
28. Sherman-Baust CA, Kuhn E, Valle BL, Shih Ie M, Kurman RJ, Wang TL, et al. A genetically engineered ovarian cancer mouse model based on fallopian tube transformation mimics human high-grade serous carcinoma development. J Pathol 2014;233:228–37.
29. Connolly DC, Bao R, Nikitin AY, Stephens KC, Poole TW, Hua X, et al. Female mice chimeric for expression of the Simian Virus 40 TAg under control of the MISIIR promoter develop epithelial ovarian cancer. Cancer Res 2003;63:1389–97.
30. Köbel M, Kalloger SE, Boyd N, McKinney S, Mehl E, Palmer C, et al. Ovarian carcinoma subtypes are different diseases: Implications for biomarker studies. PLoS Med 2008;5:e232.
31. Tsai SQ, Zheng Z, Nguyen NT, Liebers M, Topkar VV, Thapar V, et al. GUIDE-seq enables genome-wide profiling of off-target cleavage by CRISPR-Cas nucleases. Nat Biotechnol 2015;33:187–97.
32. Kim D, Bae S, Park J, Kim E, Kim S, Yu HR, et al. Digenome-seq: genome-wide profiling of CRISPR-Cas9 off-target effects in human cells. Nat Methods 2015;12:237–43, 1 p following 43.
33. Tang X, Asano M, O'Reilly A, Farquhar A, Yang Y, Amar S. p53 is an important regulator of CCL2 gene expression. Curr Mol Med 2012; 12:929–43.
34. Tang X, Amar S. p53 suppresses CCL2-induced subcutaneous tumor xenograft. Tumour Biol 2015;36:2801–8.
35. Movahedi K, Guilliams M, Van den Bossche J, Van den Bergh R, Gysemans C, Beschin A, et al. Identification of discrete tumor-induced myeloid-derived suppressor cell subpopulations with distinct T cell-suppressive activity. Blood 2008;111:4233–44.
36. Candido Dos Reis FJ, Song H, Goode EL, Cunningham JM, Fridley BL, Larson MC, et al. Germline mutation in BRCA1 or BRCA2 and ten-year survival for women diagnosed with epithelial ovarian cancer. Clin Cancer Res 2015;21:652–7.